Efficient Multidisciplinary Analysis Approach for Conceptual Design of Aircraft with Large Shape Change

Pawel Chwalowski, Jamshid A. Samareh, Lucas G. Horta, David J. Piatak,

Anna-Maria R. McGowan
NASA Langley Research Center
Hampton, VA 23681

Pawel.Chwalowski-1@nasa.gov

ABSTRACT

The conceptual and preliminary design processes for aircraft with large shape changes are generally difficult and time-consuming, and the processes are often customized for a specific shape change concept to streamline the vehicle design effort. Accordingly, several existing reports show excellent results of assessing a particular shape change concept or perturbations of a concept. The goal of the current effort was to develop a multidisciplinary analysis tool and process that would enable an aircraft designer to assess several very different morphing concepts early in the design phase and yet obtain second-order performance results so that design decisions can be made with better confidence. The approach uses an efficient parametric model formulation that allows automatic model generation for systems undergoing radical shape changes as a function of aerodynamic parameters, geometry parameters, and shape change parameters. In contrast to other more self-contained approaches, the approach utilizes off-the-shelf analysis modules to reduce development time and to make it accessible to many users. Because the analysis is loosely coupled, discipline modules like a multibody code can be easily swapped for other modules with similar capabilities. One of the advantages of this loosely coupled system is the ability to use the medium- to high-fidelity tools early in the design stages when the information can significantly influence and improve overall vehicle design. Data transfer among the analysis modules are based on an accurate and automated general purpose data transfer tool. In general, setup time for the integrated system presented in this paper is 2-4 days for simple shape change concepts and 1-2 weeks for more mechanically complicated concepts. Some of the key elements briefly described in the paper include parametric model development, aerodynamic database generation, multibody analysis, and the required software modules as well as examples for a telescoping wing, a folding wing, and a bat-like wing. The paper also includes the verification of a medium-fidelity aerodynamic tool used for the aerodynamic database generation with a steady and unsteady high-fidelity CFD analysis tool for a folding wing example.

1.0   INTRODUCTION

All aircraft undergo some degree of shape change to accomplish their mission. This is commonly achieved by moving control surfaces. However, several aircraft have exhibited larger than normal shape changes that include variable sweep, variable span, and/or folding wing concepts. Some of the early research aircraft that exhibited large-shape change included the X-5, XB-70 Valkyrie, and the oblique wing. Operational aircraft that have had the ability to change their shape significantly during their mission include the B-1 Lancer, F-8,

F-111, F-14, Mirage G, MiG-23, MiG-27, and Sukhoi Su-17. In each of these examples, the specified mission was more diverse or broader than conventional design, driving the wing design to a highly reconfigurable or large-shape change concept. Large-shape change concepts nearly always have associated design "penalties" such as added weight or complexity. However, when overall system performance and mission requirements are assessed, large-shape change concepts can be a viable approach for some missions - particularly missions that may be described as combinations of several missions with diverse speed, altitude, or take-off and landing requirements.

Over the past decade, several research efforts have focused on developing or assessing a new breed of multi-mission aircraft and related innovative technologies that include large shape change[1]. Technologies that can address multi-mission requirements range[2] from little or no shape-change, such as micro flow control and variable bumps[3] to moderate shape change such as variable airfoil shape (including camber change[4]) and wing twist[5]; to large scale shape[6] change such as variable span[7], sweep[8], and fold angle[9]. In the literature, this suite of technologies has many names including: reconfigurable, multifunctional, adaptive, or morphing technologies. This report will refer to advanced technologies that may address multi-mission requirements as "morphing." Morphing may also be defined as efficient, multi-point adaptability. Technological advances and innovation in several fields, such as materials, structures, aeroelasticity, flow control, aerodynamics, and flight control, have enabled many of these novel morphing concepts to come closer to reality for aircraft in the 21st century.

With potential new capabilities in hand, today's aircraft designer has new opportunities as well as new challenges, for the promises of morphing benefits are not without a penalty. Shape change typically requires additional hardware, weight, and/or complexity. One major weight penalty is the additional actuator weight, which is a function of the mechanisms used and the energy required to morph. Another design challenge is determining which technology or technologies to use for shape change, whether it is for little or no shape change or large shape change. Designers of morphing vehicles must also optimize the use of the technologies or suite of technologies and conduct trade-off studies to weigh benefits and penalties. The system benefits must significantly outweigh the penalties for the new morphing concept to survive the conceptual design phase. Further assessment of shape-change concepts requires analysis of the air vehicle at different flight conditions and shapes, and each condition may require a different analysis model (e.g., aerodynamic mesh). Analysis models for small and moderate shape changes can be generated with slight modifications of the un-morphed analysis models. However, analysis models for large-scale shape changes may need to be regenerated for every morphed stage. This time-consuming model regeneration process often precludes conducting multiple analyses early in the design stage (during conceptual design) unless the process is automated for different morphing stages. Yet, conceptual design phase is where the aircraft designer has greatest flexibility to trade a variety of shape-change concepts. Unfortunately, due to the complexities mentioned previously, many conceptual design efforts using morphing concepts tend to focus on perturbations about one particular type of shape change concept (e.g., telescoping) and not on comparing several different concepts.

The research effort reported herein focuses on developing a capability to evaluate several diverse morphing concepts (focusing on large shape change) with higher fidelity and greater efficiency. This approach essentially blends some of the tools normally associated with preliminary design (such as second-order performance analysis) with the efficiency and flexibility normally associated with conceptual design. This was achieved by integrating several existing analysis capabilities, which addressed some of the common challenges with multidisciplinary analysis (MDA) for morphing aircraft. In bringing these analysis capabilities together, the authors found that the initial set-up was the most time consuming part of the process, because we had to understand the assumptions and limitations of the different analytical tools. Once this was

accomplished, the exercise of assessing a new morphing concept and getting second order performance results (e.g., loads, roll, and roll rate) was extremely quick - typically only a few days. This process would normally take months using the conventional preliminary design approach.

In this paper, the overall MDA design approach is demonstrated as well as a detailed description of each component of the design: model generation, data transfer, aerodynamic database generation, and multibody analysis. To evaluate the integrated design approach described herein, three generic and diverse shape change configurations were analyzed, and the results are provided for reference and comparison.

2.0   MULTIDISCIPLINARY ANALYSIS (MDA) FOR AIRCRAFT WITH LARGE-SHAPE CHANGES

Design and assessment of reconfigurable aircraft introduce several challenges in the conceptual[10] and preliminary design phases. Even for more traditional design approaches, stepping through the process of developing the simple sketches that initiate a conceptual design and completing the detailed analysis of a preliminary design can be very costly and time-consuming. Though preliminary design typically results in a better understanding of the benefits and penalties of a particular concept design, at this point in the design process, it is often too late to make significant changes to the design. During the NASA Morphing Program and the DARPA Morphing Aircraft Structures (MAS) program, a common question was frequently posed: "How can we quickly assess several different morphing concepts without having to spend considerable resources and time doing a detailed design for each concept?" Several challenges were identified and are described below. The current research effort was focused on addressing some of the challenges to enable a user-friendly, medium-fidelity, and yet time-efficient approach to MDA for aircraft with large shape changes. This approach is centered on automating time-consuming steps, using existing off-the-shelf software modules, and integrating these modules in a loosely coupled manner. This way, aircraft designers can use their existing tools along with this integrated tool for a rapid assessment of the types of and the amount of shape change that would address multi-mission requirements.

 One of the classic challenges of MDA is increasing fidelity while maintaining or increasing the number of disciplines and addressing the efficient and accurate data transfer among disciplines. Typically, it is very time-consuming and can be tedious to address all of these requirements because multiple models from different disciplines must be generated that include an appropriate level of physics and geometry characteristics. In addition, multi-point optimization may require multiple models for the aerodynamic analysis and structures. Morphing concepts may also require additional non-traditional disciplines such as multibody analysis (included in this study) or kinematics, etc. Thus, model generation for MDA of morphing concepts can be a significant challenge. Correspondingly, accurately moving data between the different disciplines is complex and often done in an ad-hoc manner, with no consideration for constraints such as conservation of forces, moment, and virtual work. An additional complication for vehicles with large shape change is that the uniqueness of the configuration often drives MDA analysts to develop a special-purpose tool (e.g. finite element analysis) to analyze the different shape changes. This special-purpose tool then uses a customized geometry description of a specific morphing concept. While this approach usually yields excellent results, analyzing a different concept requires a substantial change to the system. In addition, this leads to comparing different morphing concepts with different analysis systems, introducing inconsistency in the results. To address these challenges several steps were taken in the current study:

1. We have used a parameterized model with a few critical design parameters describing the geometry, flight conditions, and the morphing concepts. This parameterization allows one to analyze a diverse set of shape change concepts and enables automation of model generation and analysis. In the examples reported herein, an automated aerodynamic analysis was developed and integrated. In addition, automated finite element model generation and analysis were developed but not integrated[11].

2. We used a general-purpose validated data transfer tool that is accurate and fully automated. This capability simplified the integration process[11].

3. We used a loosely coupled integration method, which enables interchangeability of software modules with similar capabilities and allows the use of up-to-date analysis modules. In addition, the software modules are encapsulated and there is no need to modify them. This also enables the use of off-the-shelf software and the inclusion of more disciplines. In our examples, we were able to compare the results of two different multibody codes[11].

4. We used off-the-shelf software modules to accelerate our development process. This put an additional burden on the initial integration effort. However, we believe this burden is a worthwhile effort as we were able to avoid writing large pieces of software and gained flexibility in being able to include different codes[11].

5. We have verified the accuracy of the medium-fidelity aerodynamic tool used for this study. The verification was accomplished with the high-fidelity computational fluid dynamic (CFD) software for the folding wing concept. The steady and time-dependant aerodynamic analysis of the folding wing concept showed that there is no need for a high-fidelity, time-dependent aerodynamic analysis at slow morphing speeds.

The overall integrated approach is capable of analyzing a diverse set of morphing concepts, hence eliminating any inconsistency due to dissimilar and disparate systems. Figure 1 shows our integrated approach for design and analysis of morphing concepts. The approach includes geometry generation, aerodynamic analysis, structural analysis, multibody analysis, and data transfer among various disciplines. Modules for structural model generation and analysis have been developed, but they have not been integrated yet. The commercial software MATLAB® (MathWorks*) is used to generate the aerodynamic meshes; Discrete Data Transfer Between Dissimilar Meshes (DDTBDM[12]) is used to transfer data among aerodynamics, structures, and the multibody dynamics models; Virtual Lab® (LMS†) and DYMORE[13] are used for dynamics analysis; and CMARC® (AeroLogic‡) is used for aerodynamics analysis. This is a loosely coupled integrated analysis, and one can easily swap any of these modules with other software modules with similar capabilities.

---

* MATLAB is a trademark of Math Works (http://www.mathworks.com)

† Virtual Lab is a trademark of LMS International (http://www.lmsintl.com)

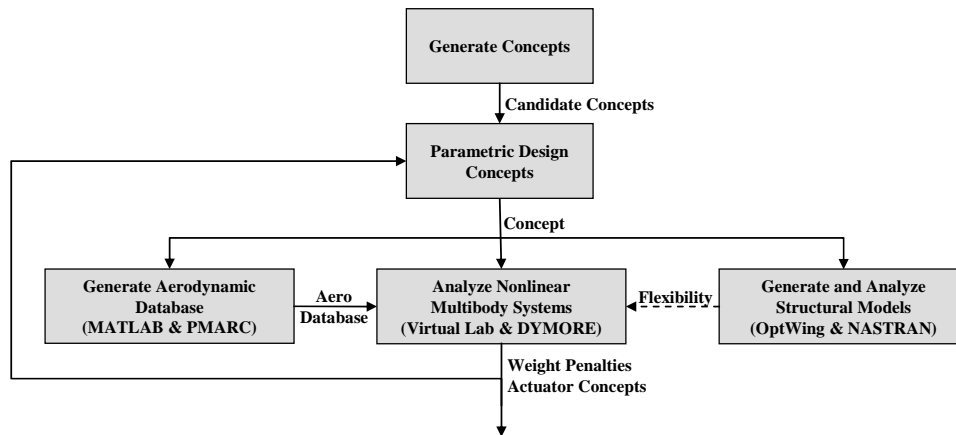‡ CMARC is a trademark of AeroLogic (http://www.aerologic.com)

Figure 1: Overall design process.

3.0   PARAMETRIC MODEL GENERATION

The use of parametric models is an essential element of our approach. It allows for simplification and automation of the model generation for a diverse set of morphing concepts. The parametric model is based on a wing, which is decomposed into several panels. Each panel is parameterized as shown in Fig. 2 with five variables: 1) root chord C_r, tip chord C_t, aspect ratio AR, quarter-chord sweep angle λ, and wing fold angle θ.

With this set of parameters, it is possible to generate a large number of morphing wings including the three examples shown in Fig. 3. Tables 1-3 show the parameters used in our examples and Figs. 4-5 show the wing planforms. Table 4 shows the mass and inertia properties for the telescoping, folding, and bat-like wings, and these wings are sized to be consistent with empirical vehicle sizes.
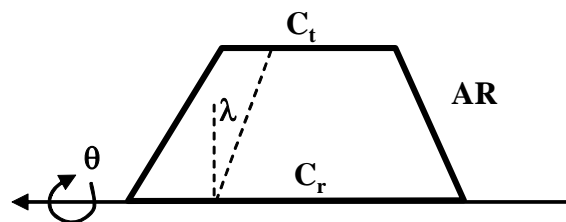
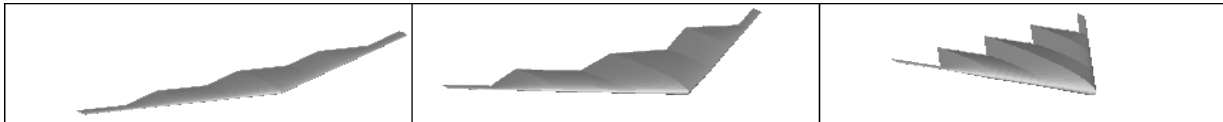**Figure 2: Geometry parameterization for one panel.**
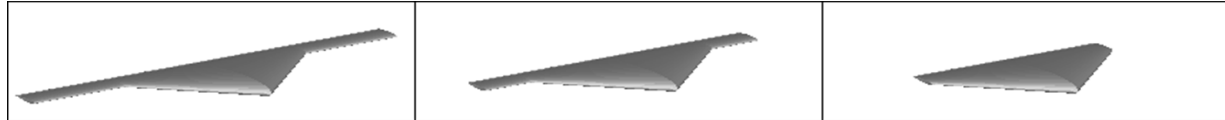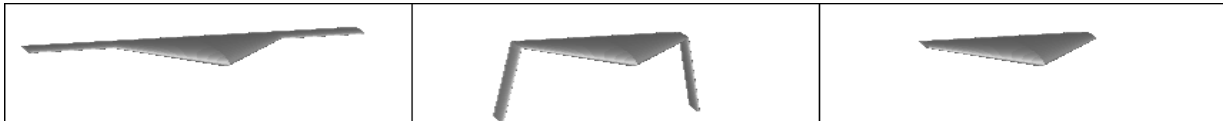
a) Telescoping wing

b) Folding wing

c) Bat-like wing

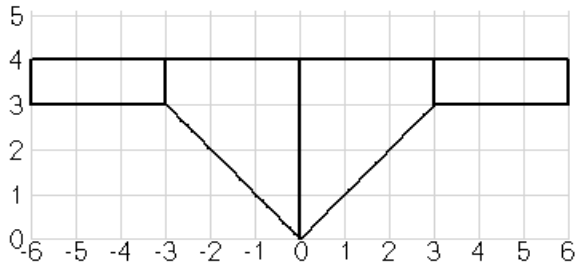**Figure 3: Sample morphing wings (left: un-morphed, middle: 50% morphed, right: fully-morphed).**

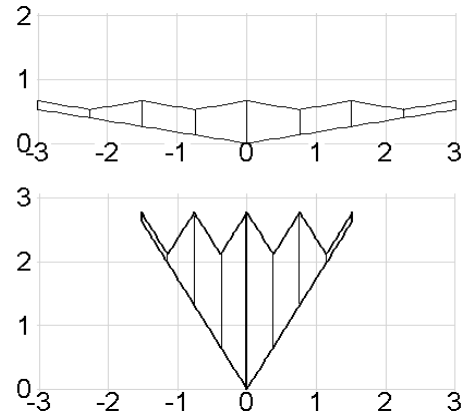**Figure 4: Planform view of telescoping and folding wings.**

Figure 5: Planform view of bat-like wing

Telescoping Wing				
	Initial		Final	
Panel #	1	2	1	2
Cr(meter)	4	1	4	1
Ct(meter)	1	1	1	1
AR	1.2	**0**	1.2	**3**
λ (deg)	37	0	37	0
Fold Angle (deg)	0	0	0	0
Ref. Chord (m)	4			
Ref. semi-span (m)	3			
Ref. Area (m^2)	7.5			
λ is the quarter-chord sweep angle				

Table 1: Telescoping wing

Folding Wing				
		Initial		Final
Panel #	1	2	1	2
Cr(meter)	4	1	4	1
Ct(meter)	1	1	1	1
AR	1.2	3	1.2	3
λ (deg)	37	0	37	0
Fold Angle (deg)	0	**0**	0	**180**
Ref. Chord (m)	4			
Ref. semi-span (m)	6			
Ref. Area (m^2)	10.5			

Table 2: Folding wing parameters.

Bat Wing								
	Initial				Final			
Panel #	1	2	3	4	1	2	3	4
Cr(meter)	0.66	0.4	0.4	0.13	2.77	1.45	1.45	0.13
Ct(meter)	0.4	0.4	0.13	0.13	1.45	1.45	0.13	0.13
AR	1.42	1.89	2.84	5.67	0.18	0.26	0.48	2.89
λ (deg)	5.04	10	5.04	10	40.9	60	40.9	60
Fold Angle (deg)	0	0	0	0	0	0	0	0
Ref. Chord (m)	0.66							
Ref. semi-span (m)	3							
Ref. Area (m^2)	1.986							

Table 3: Bat-like wing parameters.

		Mass, kg	Ixx, kg-m^2	Iyy, kg-m^2	Izz, kg-m^2
Telescoping and Folding Wings	Center Body	985.13	1191.2	3176.1	2119.5
	Outer Wing	58.7	44.5	0.75	44.5
Bat-like Wing (10° deg Configuration)		985.13	1191.2	3176.1	2119.5

Table 4: Mass and inertia properties of telescoping, folding, and bat-like wings.

4.0 DATA TRANSFER AMONG DISCIPLINES

Accurate and automated data transfer among various disciplines is a key ingredient for the loosely coupled analysis and design process. Often discipline models share the same geometry, but the models (e.g., aerodynamics and structures) have dissimilar meshes. In addition, the data transfer process between disciplines may be subject to additional constraints, such as conservation of forces, moments, and energy. One source of error often occurs when models have dissimilar levels of geometry details. For example, an aerodynamic mesh generally resembles the true geometry of the aircraft; the mesh includes details such as pylons, nacelles, flaps, and slats. However, a structural mesh generally represents only the major structural modules, such as a wing box, but flaps and slats either are represented as simple beam elements or are completely excluded.

The work by Samareh[12] provides a general algorithm for data transfer that is accurate and satisfies the required constraints. Figure 6 shows the results of load transfer for a morphing configuration: (a) aerodynamic mesh, (b) coefficients of pressure on the aerodynamic mesh, (c) load vectors on the aerodynamic mesh, (d) a simple mesh for multibody analysis (colors corresponds to different wing panels), and (e) transferred load vectors on the multibody mesh. The load transfer process used in this study is accurate and guarantees conservation of forces and moments.
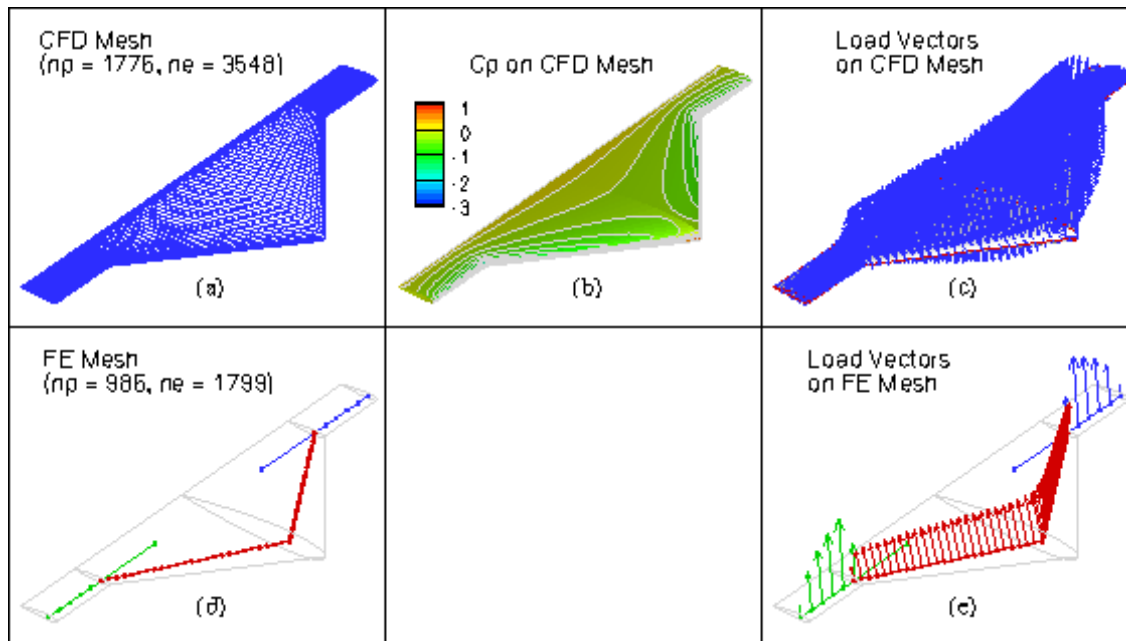

Figure 6: Load transfer for a morphing vehicle.

5.0 AERODYNAMIC DATABASE GENERATION

One key assumption in creating the aerodynamic database is that the shape changes occur at much slower rate than the free stream velocity. This assumption allows one to use a series of steady aerodynamic solutions to model the flow field. For this, MATLAB based software coupled with the potential flow aerodynamic code CMARC is used. MATLAB is a high performance software application for engineering and scientific

computation and visualization, and CMARC code is a commercial version of the potential-flow panel method code, PMARC[14], developed at NASA Ames. The CMARC code is capable of calculating the surface pressure distribution around a 3-dimensional body, assuming that the flow field is incompressible, inviscid, and irrotational. It also has the capability to calculate skin friction over the wing; however, this capability was not used for this study. This section presents the process of aerodynamic mesh generation, CMARC execution, and aerodynamic database generation. The process can be easily extended for aerodynamic analysis based on computational fluid dynamics (CFD).

```
#WING CREATION INPUT DECK
#number of sections
4
#root chord lengths
0.66 0.4 0.4 0.13
#tip chord lengths
0.4 0.4 0.13 0.13
#Aspect Ratios
1.42 1.89 2.84 5.67
#Quarter Sweep Angles (degrees)
5.04 10.0 5.04 10.0
#Number of panels comprising each wing
10 10 10 10
#Fold angles (degrees)
0.0 0.0 0.0 0.0
#Spline points
25
#Wing configuration option (1 full, 2 half)
1
#Solver type option (1 CMARC, 2 Vorview)
1
#Units option (2 for English (feet), 1 for Metric)
1
#Mach number (For flow solver)
0.2
#Alpha schedule vector (For flow solver)
-10 -5 0 5 10
#Reynolds number based on chord and dimensional kinematic viscosity
480000  0.0001
#File consisting of airfoil point definition
naca0012.dat
```

Figure 7: Bat-like wing planform and sample input script for MATLAB script to generate bat wing geometry.

The aerodynamic database used in this study has as input variables the angle of attack and geometric parameters describing the morphing shape changes. These geometric parameters controlling the shape changes are the retraction distance for the telescoping wing, a folding angle for the folding wing, or a leading-edge sweep angle for the bat-like wing. Outputs from the aerodynamic database consist of forces and moments acting at discrete points on the wing. It is at these discrete points that the multibody dynamic analysis model (mesh) accepts external loads. For example, for DYMORE[13] models, the discrete points in the database are

located along the wing quarter-chord line for the telescoping wing. For LMS Virtual Lab models, the discrete points are located on the leading and the trailing edges of the wing.

Figure 7 shows a planform view of a bat-like in-plane morphing wing similar to concepts developed by NextGen Aeronautics[§] and a sample input script required by MATLAB. This input script describes four-section bat-like wing geometry with corresponding root chord, tip chord, aspect ratios, quarter-chord sweep angles, and fold angles between each section. For the example shown in Fig. 7, each wing section has 10 panels in the spanwise direction. There are 50 points (25 points on the top and 25 on the bottom) per airfoil section and the wing configuration option allows for full-wing geometry or half-wing geometry to be executed in CMARC. Based on this input, the MATLAB script generates a surface mesh in the format required by CMARC. This MATLAB script offers great flexibility to change any or all the geometric parameters and to generate CMARC solutions quickly, without user interaction, for a vehicle with large shape changes.

In addition to CMARC, the MATLAB script has a link to a vortex lattice code called Vorview[15] (an option available in the input script under solver type option). The MATLAB script reads the variables describing the initial and the final morphing shapes from the geometry input deck and linearly interpolates for the intermediate shapes from the initial and the final values of leading edge sweep angles. Then, MATLAB creates a CMARC mesh and invokes CMARC to obtain the aerodynamic solution. Figure 8 shows sample mesh and surface pressure solution results for the bat-like wing shown in Fig. 7. It took one second to generate
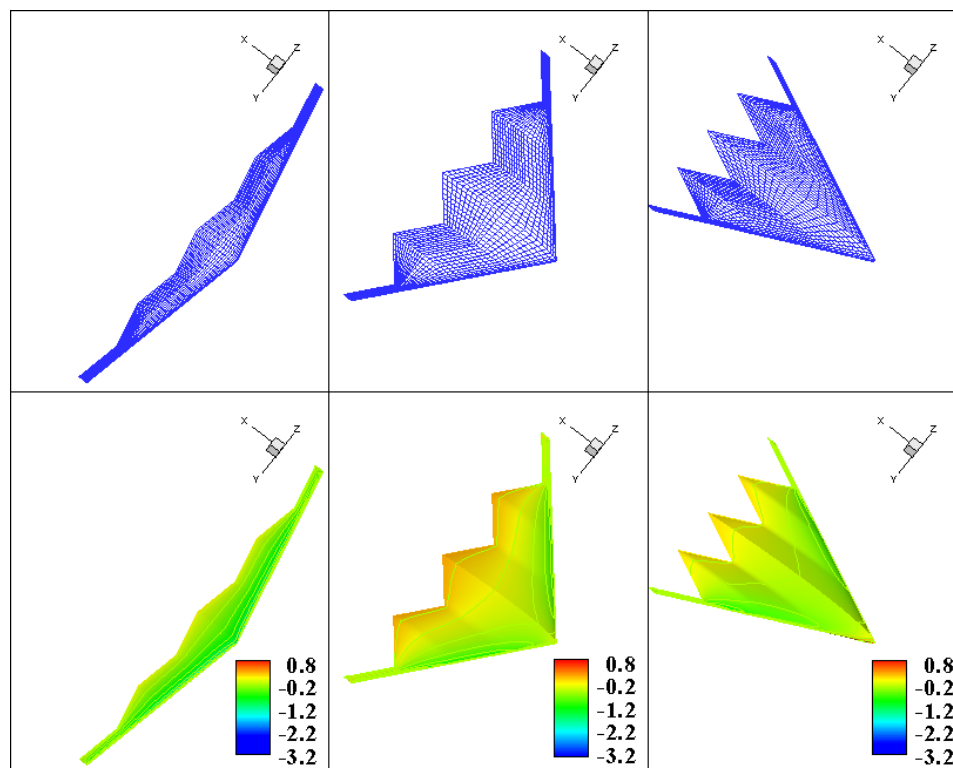
Figure 8: Mesh and coefficients of pressure for a bat-like wing.
(Left: un-morphed, middle: 50% morphed, right: fully-morphed).

[§] http://www.nextgenaero.com

each mesh and 11 seconds to generate each CMARC solution on a 3.2 GHz PC running Linux OS.

6.0 AERODYNAMIC DATABASE VERIFICATION

CMARC aerodynamic analysis software was used to create the aerodynamic database for all three morphing wing concepts. CMARC solves potential flow equations, and solving these equations is essential in reducing the computational requirements and enabling automation of the aerodynamic analysis process. However, these solutions could also introduce unacceptable errors in the aerodynamic predictions. In the current study, these errors could be due to the absence of viscous effects and the assumption of steady state aerodynamics.

The Fully Unstructured Navier-Stokes 3-Dimemsional, FUN3D[16], was used to verify the accuracy of our CMARC-based aerodynamic database. In addition to many standard options, FUN3D includes various time-varying mesh deformation and moving body schemes applicable to the current study[17]. This study used the time-varying mesh deformation scheme to verify the CMARC results for the folding wing example as shown in Fig. 3b. The scheme uses the time dependent mesh surface to adjust the volume grid.

The CFD analysis of the folding wing, both steady state and unsteady, consisted of inviscid (Euler) and viscous analyses. The inviscid volume grid had approximately 1.2 million nodes, and the viscous volume grid had approximately 9 million nodes with a fully gridded boundary layer with the first cell height of y^+=1. The Spalart-Allmaras (SA) turbulence model was used in the viscous analysis. The effects of grid resolution and turbulence model were not included in the study. The unstructured grids were generated using VGRID[18] software.

6.1 Folding Wing: Steady-State Analysis Results

Both inviscid and viscous steady-state solutions of the folding wing were computed at 0° and 90° fold angles for various angles of attack. The computed aerodynamic coefficients at 0° and 90° fold angles are shown in Figs. 9 and 10, respectively. The results show a good agreement between CMARC and FUN3D aerodynamic predictions. In fact, there is a very little difference in lift and pitching moment coefficients between FUN3D Euler and CMARC results. The largest differences are computed at either 10° or -10° angles of attack. As expected, the coefficient of drag is under predicted using the CMARC code by approximately a factor of two. This is a reasonable prediction, because CMARC can only approximate an induced drag that averages about 40 percent of the total drag. Also, FUN3D solutions show that the viscous drag is a small part of the total drag. However, grid convergence and turbulence model effects on drag predictions were not included in this work. Figure 11 shows coefficient of pressures, Cp, on top and bottom surfaces at 5° and 10° angles of attack for 0° and 90° fold angles. Similar Cp contours are computed using CMARC and FUN3D. However, FUN3D computes a vortex shedding due to the sharp corner where the wing's cord length transitions to a constant value. Even though the CMARC code cannot predict the vortex shedding, the integrated aerodynamic coefficient values are not greatly affected.
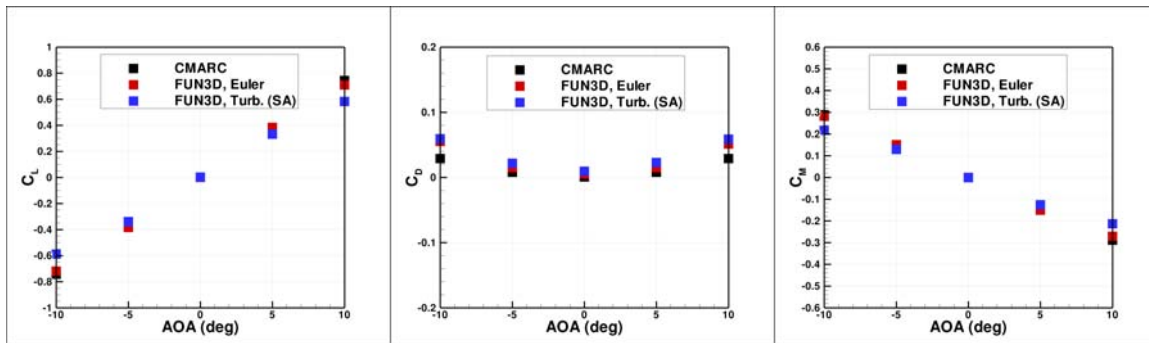
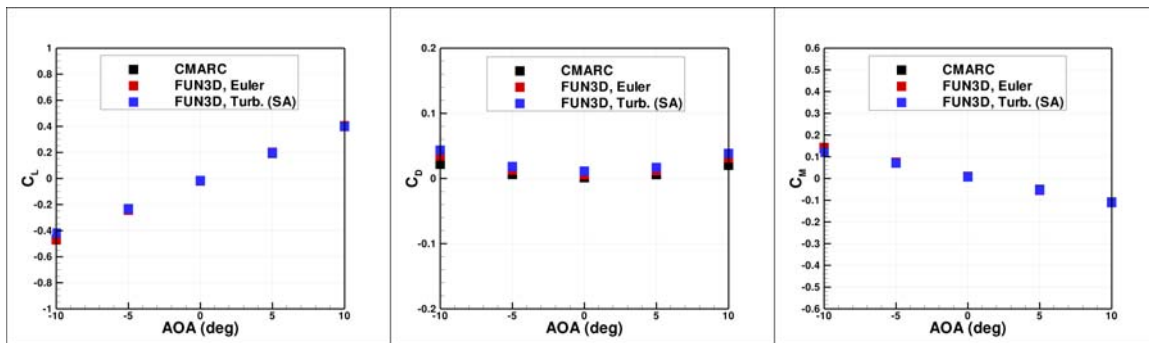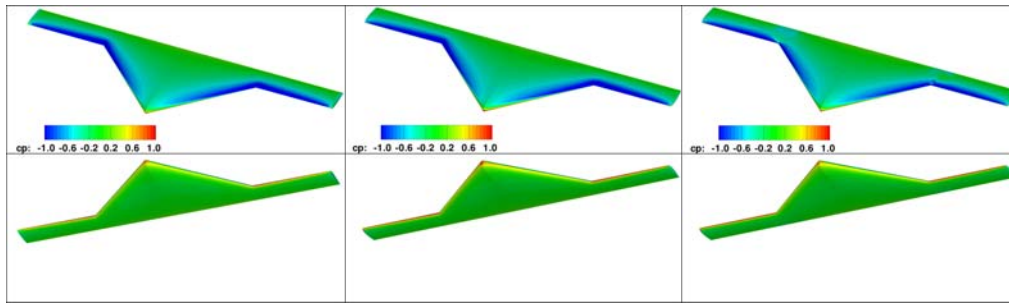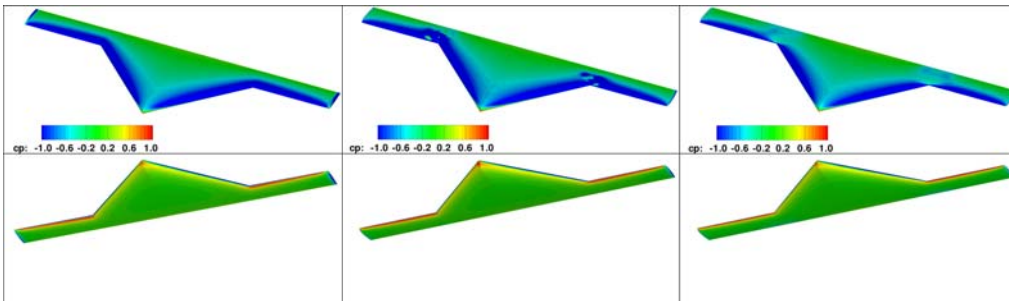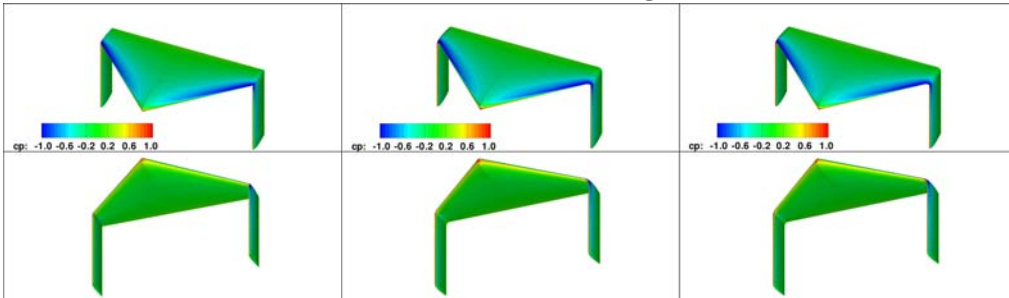**Figure 9: Aerodynamic coefficients computed at 0° fold angle.**

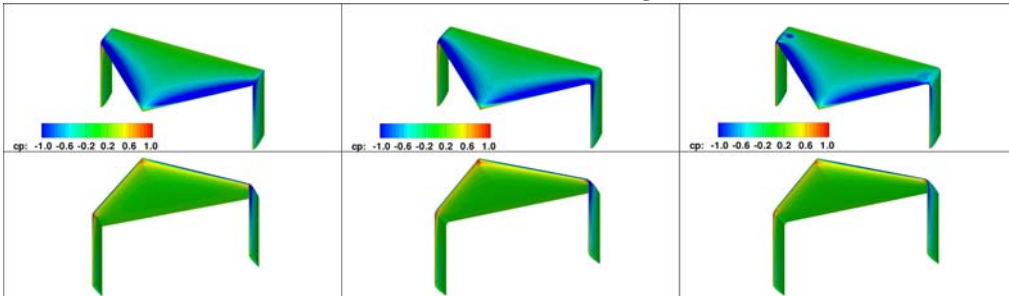**Figure 10: Aerodynamic coefficients computed at 90° fold angle.**

(a) 5° AOA and 0° fold angle

(b) 10° AOA and 0° fold angle

(c) 5° AOA and 90° fold angle

(d) 10° AOA and 90° fold angle

**Figure 11: Comparison of surface pressure coefficients Cp: CMARC (left), FUN3D
Euler (middle), FUN3D Turbulent (right).**

6.2 Folding Wing: Unsteady FUN3D Analysis Results

The 0° fold angle grid and its corresponding steady state flow field were used as initial conditions for the unsteady FUN3D analysis. In the unsteady analysis a series of the time varying surface meshes is generated external to FUN3D. The surface meshes are based on the initial surface mesh node topology. To fold the surface mesh, a grid folding algorithm was developed where the location of the stationary, folding, and rotating regions are specified. The FUN3D code automatically deforms the volume grid based on each deformed surface mesh. Each deformed surface mesh has a time stamp associated with the wing fold rotation angle, which allows for specification of the wing fold speed. In this analysis, two wing fold speeds are analyzed: 1deg/sec and 5deg/sec. The 1deg/sec and 5deg/sec wing rotation speeds imply that it takes 180 and 36 seconds, respectively, to fold the entire wing. Because the computational time step is significantly smaller than the folding time, FUN3D automatically interpolates surface meshes and deforms the volume grid based on the global time. The unsteady computations are performed at 10° angle of attack. At this angle of attack, the largest differences between inviscid and viscous steady state results were observed.

Figure 12 shows the cut through the volume grid used in the inviscid analysis at the initial 0° and intermediate 80° fold angle positions. This figure demonstrates that the grid distribution in the volume grid is consistent between the initial and the intermediate folding locations. This is evidenced by a similar grid distribution without excessive grid concentration near the wing tip and the folding location. On the other hand, the 80° fold angle requires very large mesh rotations and volume adjustments and some grid stretching under the wing is visible. In the folding wing example, the surface mesh can be rotated only 81 degrees for the inviscid case and 71 degrees for the viscous case before the volume grid regeneration in FUN3D fails due to negative volumes.
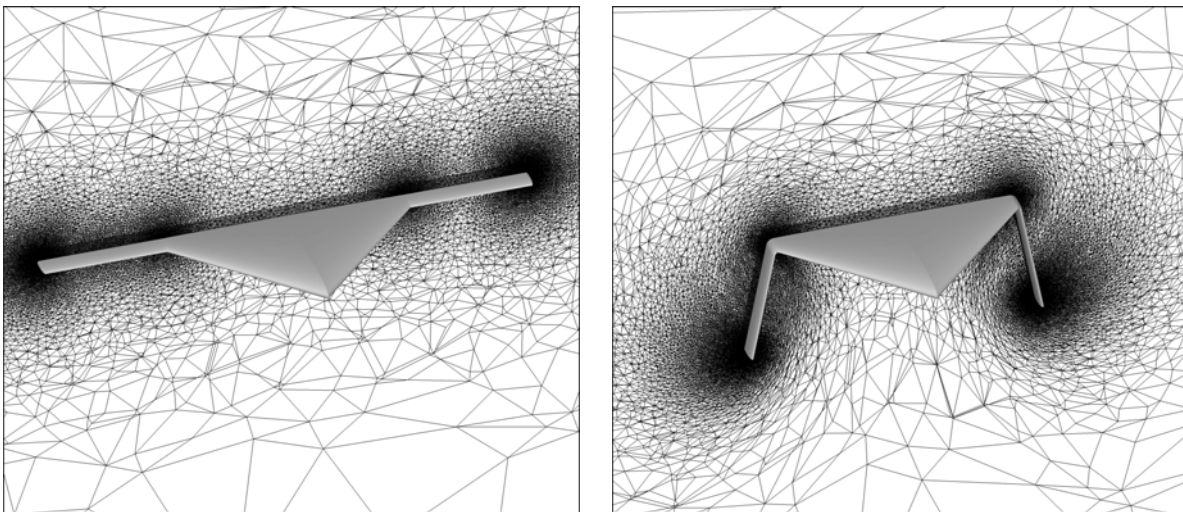

Figure 12: Cuts through the volume grid: Initial 0° (left) and 80° (right) fold angles.

In Figure 13 the aerodynamic coefficients from the unsteady analysis are plotted against the folding angle. This figure shows the results for the inviscid and viscous cases where the red, green, and blue lines show drag, pitching moment, and lift coefficients at 1deg/sec wing folding speed. The overlaid dashed black lines

represent 5deg/sec wing folding speed. The bounded color squares show the steady state results computed at selected wing fold angles. Two observations are made. First, there is negligible difference between the steady state and the unsteady results at these wing folding speeds. Therefore, the original assumption that the shape changes occur at a much slower rate than the fluid particles travelling across the wing chord is correct. Second, the vortex shedding, characterized by small scale fluctuations in aerodynamic coefficients, seems to diminish as a fold angle becomes greater. The vortex shedding is a local effect and does not significantly affect global aerodynamic trends. Figure 14 compares the inviscid (I) and viscous (V) unsteady solutions. The difference between the inviscid and viscous solutions remains relatively constant throughout the unsteady simulation.
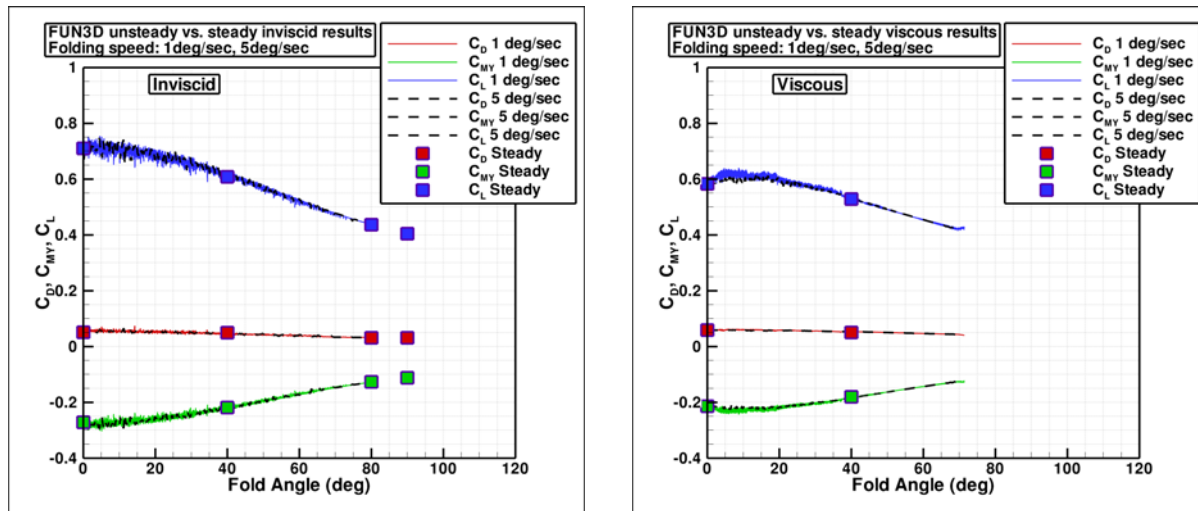
Figure 13: Unsteady FUN3D results: inviscid (left), viscous (right).
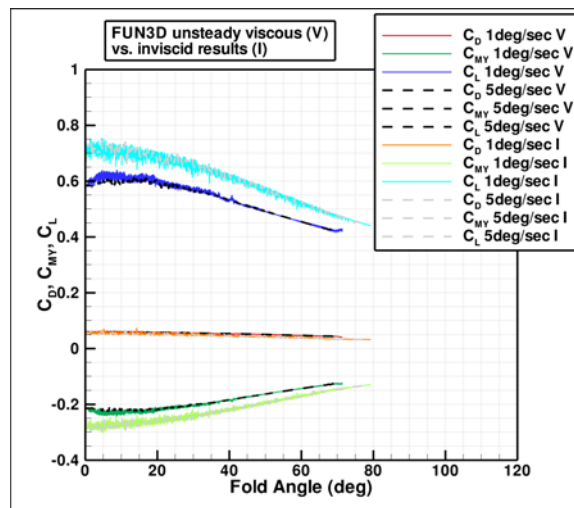
Figure 14: Comparison of inviscid and viscous solutions.

Both inviscid and viscous volume grids were split into 128 partitions. It took approximately 30 minutes to generate the inviscid grid and two hours to generate the viscous grid on a single processor (Intel Xeon 5100). It took 16 minutes to obtain a single inviscid steady-state solution and five hours to obtain a single viscous steady-state solution. In contrast, it took only 1 second to generate each mesh and 11 seconds to generate each CMARC solution on a 3.2 GHz PC running Linux OS. It took 46 hours to obtain the unsteady FUN3D solution on an inviscid grid and 227 hours on a viscous grid. The aerodynamic results and the computational time suggest that at the slow folding rates there is a minimal benefit in using high-fidelity flow analysis for a folding wing concept.

7.0 MULTIBODY DYNAMICS ANALYSIS

Classical finite element-based structural analysis methods have proven to be robust design tools for the determination of static, dynamic, aeroelastic, and aeroservoelastic response of conventional aircraft configurations. However, the structural and aeroelastic analysis of morphing vehicles capable of radical shape changes require tools that enable the modeling of integrated mechanisms, structures, controls, and aerodynamic forces. Also important is the ability to analyze a complete virtual aero-structural morphing system across its full dynamic range of motion with large geometric and structural deformations without having to develop time consuming finite element models of a succession of intermediate morphed configurations. Existing multibody dynamic analyses offer the ability to model integrated aero-structural-control characteristics of morphing vehicles in the time domain when coupled with an aerodynamic model to aid in rapid prototyping and design optimization of various morphing concepts. This paper focuses on the use of two multibody dynamic analysis codes known as LMS Virtual Lab (VL) and DYMORE.

7.1 LMS Virtual Lab and MATLAB Simulink Implementation

To create the VL model for both folding and telescoping configurations, the outer mold line is read in from the computer-aided design (CAD) geometry, which was generated by the geometry process. Each moving surface, like the right and left wing, is modeled as an independent body connected using joints. For a telescoping wing concept, a translational joint is used to connect each wing-section to the center body. For the case where the wings fold inward, a revolute joint is used instead. To incorporate external aerodynamic loads into the model, eighteen points are selected on the vehicle surface where the loads are applied, 6 on the center body and 6 on each wing panel. These aerodynamic loads act in all three directions at each point. Coupling of the multibody code with the aerodynamic loads is accomplished within the MATLAB/Simulink software environment and the co-simulation capabilities of VL. Figure 15 shows the block diagram and the model elements interconnections. To simulate the vehicle VL creates the multibody equations of motion with inputs in terms of aerodynamic forces, control surface commands, and support constraints, while MATLAB couples and integrates the equations in time to compute vehicle response. In the configuration studied, the vehicle is mounted on a pedestal free to rotate. During simulations, the desired angle of attack is reached by controlling reaction torques from the vehicle onto the mounting pedestal. Although this condition is not consistent with free flight, it is consistent with many wind tunnel tests. The aerodynamic database, on the other hand, accepts control surface commands (geometric parameters) and angle of attack values to produce the aerodynamic loads that are the feedback to the multibody model. Although it is possible to loosely couple models like this at each flight condition manually, the planform changes are so radical that this is the most efficient way to study these types of vehicles.
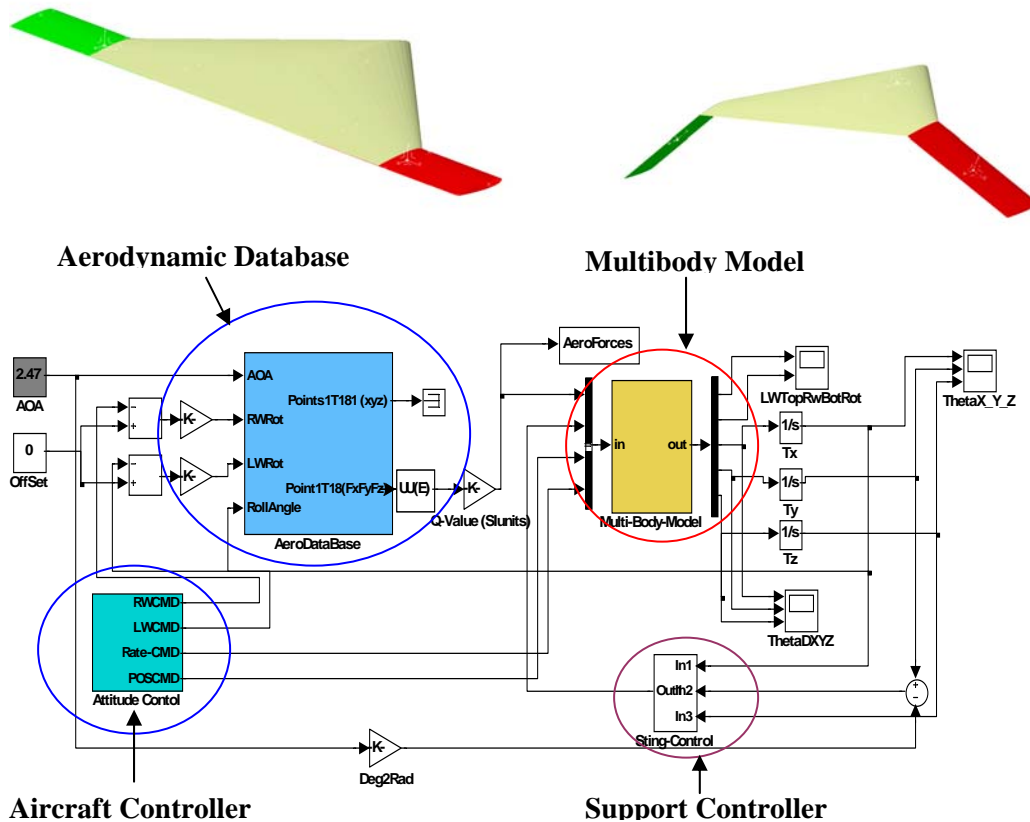
Figure 15: Simulink/Virtual Lab block diagram of telescoping and folding wing models.

7.2 DYMORE Implementation

DYMORE[13], developed by Professor Olivier Bauchau of Georgia Institute of Technology, is a finite element-based tool for the analysis of non-linear elastic multibody systems with arbitrary system topologies. The DYMORE element library consists of beams, shells, rigid bodies, joint constraints, contact joints, backlash/freeplay joints, and actuator elements. Sensors can be assigned to various elements to observe deformations, displacements, forces, and moments. Although not used in this study, DYMORE includes a state-space 2-D unsteady lifting line aerodynamic model and the ability for tight coupling of the structural model to the Navier-Stokes structured grid flow solver OVERFLOW via structured files. Aeroservoelastic problems can also be formulated within the DYMORE environment through controller elements, which couple model sensors to joint/actuator motions via linear and user-defined control law definitions. Thus, morphing mechanisms of varying degrees of complexity can be modeled using DYMORE with the inclusion of elastic, aeroelastic, and aeroservoelastic effects[19].

For the present study, DYMORE models of generic telescoping, folding, and bat-like in-plane morphing vehicle concepts have been formulated and coupled to the MATLAB steady aerodynamic database described in the previous section. Using DYMORE's Fluid Structure Interface (FSI) formatted file exchange architecture, commanded morphing displacements, rotations, MATLAB/CMARC steady forces, and moments at the quarter chord are exchanged at each time step. The structure and morphing mechanisms of the three morphing concepts described in this paper are modeled in DYMORE as beam finite elements connected by translational prismatic joints and/or rotational revolute joints. The present DYMORE models are restrained in all translational degrees of freedom, pitch, and yaw, but are allowed to rotate in roll about a revolute joint to explore the use of asymmetric morphing actuation for roll control. Although structural deflections, rotations, and velocities of beam element nodes are passed to the MATLAB aerodynamic database at each time step, these are not utilized in the steady aerodynamic database of this study but could be utilized by an unsteady aerodynamic code as part of an aeroelastic or aeroservoelastic analysis.

8.0 DISCUSSION OF SIMULATION RESULTS

This section presents the results for three wings undergoing large shape changes: telescoping wing, folding wing, and bat-like wing as shown in Fig. 3. The aerodynamic results for these three cases are presented in the Appendices A-C. For each of the three cases, the entire setup and the analysis process took approximately 3-5 days.

8.1 Telescoping Wing

To compare results from VL and DYMORE when undergoing identical shape changes, a change schedule was developed and employed within both multibody codes to produce asymmetric planform changes with 1-cos telescoping schedule. Figure 16 shows a schematic with the orientation of the joint force F_z, moment M_x, and retraction δ. Results for the telescoping concept are shown in Fig. 17; the top plot is the right wing commanded retraction that ranged from 0 to 3 meters, solid blue is VL, and dashed green is DYMORE. All results are obtained with an angle of attack of 2.47 degrees, dynamic pressure Q=2837 Pa, Mach=0.2, and 1g conditions. In order to induce vehicle roll, the right and left wing retraction commands are slightly out of phase and the

difference is shown as "$\Delta=\delta_r-\delta_l$" underneath the top plot. This command differential produced a maximum vehicle roll of 46 degrees in both simulations with a 10-12 % difference between solutions. Similarly, the predicted maximum roll rate is 3.6 deg/sec with a 10-14% difference between solutions. Another important aspect of aircraft undergoing large shape changes is joint loading. For the telescoping case, the bottom two plots in Fig. 17 show the normalized vertical shear force $F_z/(Q A_{ref})$ and torque $M_x/(Q L_{ref} A_{ref})$ at the right wing joint measured in local coordinate axes. The reference quantities are listed in Tables 1 and 4.
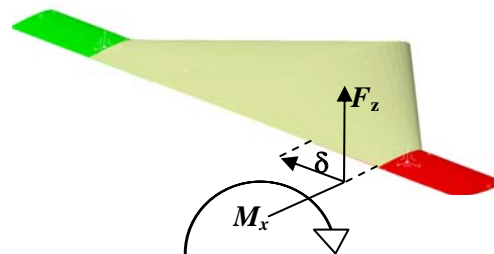
Figure 16: Free body diagram for VL and DYMORE.

When evaluating the loads, differences in the aerodynamic discretization approaches between VL and DYMORE are more apparent. For example, VL uses 6 points on each outer wing to apply the aerodynamics loads versus 11 in DYMORE. Nonetheless, the net forces and moments about the center body are the same. During telescoping the force amplitudes are modulated as the exposed wetted area is retracted inside the center body. This process introduces step discontinuities in the force and moments that are more apparent in

the VL because fewer points are used. Furthermore, because of the load discretization in VL wing forces at the junction between the right/left wing and the center body are all applied to the body side (as opposed to the wing), resulting in a step discontinuity at time zero when compared to DYMORE results. This discontinuity has little or no effect on roll and roll rate.
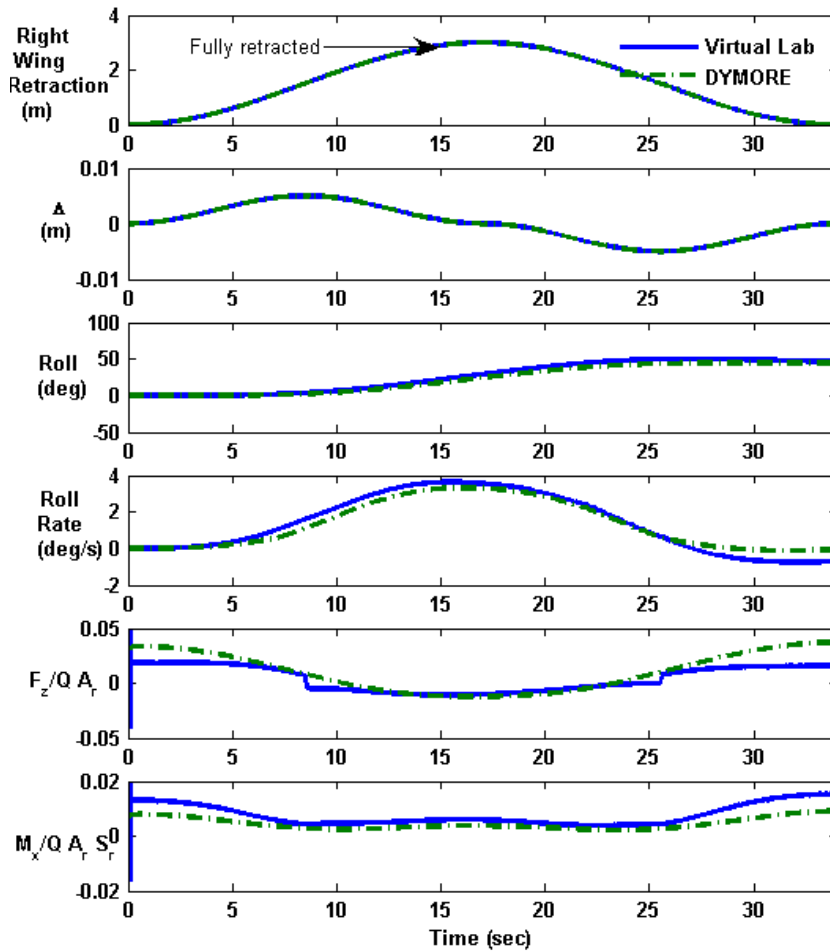

Figure 17: Comparison of telescoping wing analysis using VL and DYMORE.

8.2 Folding Wing

A folding wing concept is analyzed using a shape change schedule similar to that used in the telescoping case 1-cos function, but now the left and right wing are commanded to rotate 90 degrees in 34 seconds. At the top of Fig. 18 is the commanded rotation schedule in degrees for the right wing and under it is the difference Δ between the right and left rotation commands (Δ now used to refer to angular differences) showing a maximum difference of 1.5 degrees. Note that even this small difference causes a maximum roll of 18.8 degrees roll in DYMORE and 17.6 degrees in VL with corresponding maximum roll rates of 10.3 deg/sec and 8.65 deg/sec, respectively. Although the results from both modeling approaches are close, it is apparent that aerodynamic load discretization is the main cause of the slightly different values. When comparing normalized shear forces and actuation moments at the joint, the forces are also within the aerodynamic database load discretization error between VL and DYMORE. In addition, the spikes in the VL load plots are due to coupling of the high-bandwidth pedestal support control system used to maintain the pitch and yaw attitude during roll simulation.
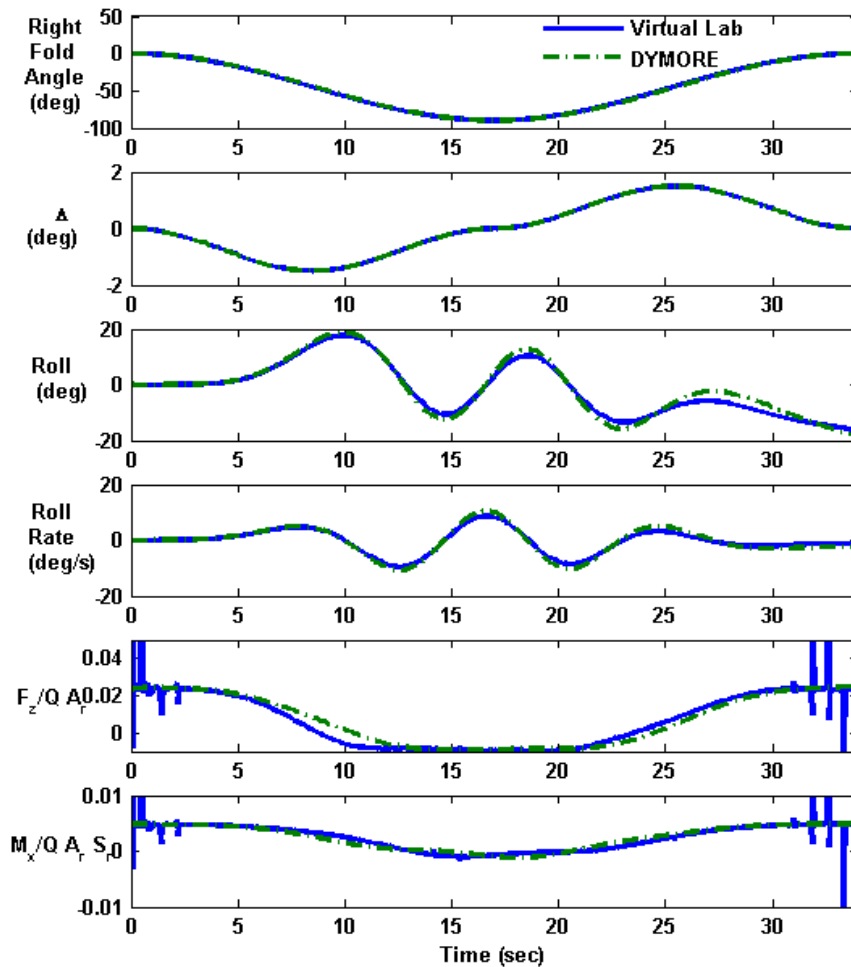

Figure 18: Comparison of folding wing analysis using DYMORE and VL.

8.3 Bat-Like Wing

A DYMORE multibody model of the bat-like wing in-plane morphing concept has been constructed and coupled to the bat-like wing aerodynamic database discussed in the previous section. Figure 19 shows the DYMORE multibody model. It also shows the connectivity of beam finite elements to revolute and prismatic sliding joints to allow the scissor-like in-plane morphing motion, which greatly affects both sweep and wing planform area. The right and left sides of the model can morph independently to allow for the investigation of asymmetric morphing commands for roll control. Results are presented in Fig. 20 for an angle of attack of 2.47 degrees, dynamic pressure Q=2837 Pa, Mach=0.2, and 1g conditions. Similar to the telescoping and folding wings, an asymmetric 1-cos schedule of leading-edge sweep angle from 10 to 60 degrees is applied as shown in the top two plots of Fig. 20, which illustrate the right wing sweep and resulting "Δ" (right wing minus left wing sweep angles).
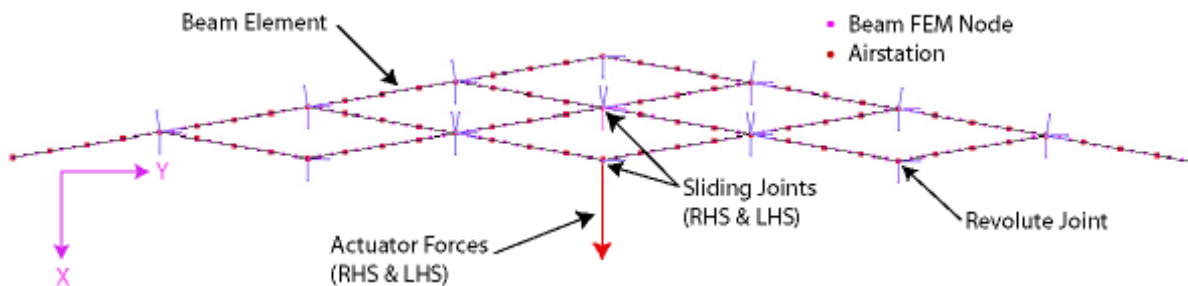
Figure 19: DYMORE multibody model of the Bat-like wing in-plane morphing concept.

Figure 20 also illustrates the resulting roll motion and roll moment due to asymmetric morphing sweep schedule. Significant residual roll velocity is present following completion of the asymmetric morphing schedule. Right and left linear actuation forces that are required to maintain right and left wing morph positions while under gravitational and aerodynamic forces are shown at the bottom of Fig. 20. These actuation forces arise due to the component of aerodynamic lift in the plane of the wing at angle of attack as illustrated in Fig. 21. Additional actuation forces would be required to overcome friction in all joints in vehicle. However, these frictional joint forces are not currently modelled in DYMORE. The results presented in Fig. 20 for the bat-like wing are to be considered preliminary, but are representative of the capabilities of the methods presented in this paper when applied to a more complex morphing concept.

Figure 21: In-plane and out-of-plane components of lift.

Figure 20: DYMORE morphing analysis of the Batwing concept.

9.0 CONCLUDING REMARKS

This paper introduced a simple, efficient, and consistent integrated approach to conduct multidisciplinary analysis for aircraft with large shape changes during the early conceptual design phase. Using a consistent set of analysis tools for several diverse morphing concepts, as opposed to using dissimilar analysis tools for each concept, provides results, which are free of any errors due to the use of different analysis tools for various concepts. The integrated approach has reduced the setup time from months to days. The approach uses model parameterization with a few critical parameters describing the geometry, flight conditions, and can handle diverse morphing concepts demonstrated with telescoping, folding, and bat-like wings. The analysis modules are loosely integrated to allow for inclusion of existing off-the-shelf analysis modules with different fidelities. For example, the use of two different multibody dynamics modules software was demonstrated, and the results show good correlation between the vehicle roll, roll rates, and critical load time histories at the joint for telescoping and folding morphing vehicle concepts. Although the two multibody simulation programs were significantly different, roll and roll rates were predicted within 10-12%. Bat-like wing results, although preliminary, illustrate the capabilities of the present analysis methods when applied to a more structurally, aerodynamically, and mechanically complex morphing concept.

Because of this study, it is clear that careful attention must be given to the distribution of aero-structural load interfaces to minimize the effects of discontinuities in aerodynamic load application for some morphing configurations. On the other hand, gross vehicle performance predictions were in good agreement even with slightly different load distributions and update rates in the multibody codes.

Aerodynamic database verification results indicated that the medium-fidelity steady-state aerodynamic method produces accurate results and there is little or no benefit in using high-fidelity, time-accurate aerodynamic analysis for a folding wing concept when wing folding rotation rates are low.

10.0 ACKNOWLEDGMENTS

11.0 APPENDIX A: AERODYNAMIC RESULTS FOR THE TELESCOPING WING

Telescoping the outer wing section has two major benefits; it reduces the wing loading, and the variable aspect ratio improves the aerodynamic performance. By adjusting the amount of telescoping, one can control the lift and drag characteristics for various missions. The planform for the telescoping model used here is shown in Fig. A1 and the corresponding parameters are listed in Tables 1 and 4. All reference quantities are based on the un-morphed shape (Tables 1 and 4). Figure A1 shows the meshes and CMARC solutions for the telescoping wing at different stages of morphing. As described in section 5.0, MATLAB is used to interpolate the aspect ratio of the outer wing section from its initial and final values. Then, MATLAB creates the aerodynamic database as a function of the angle of attack and the telescoping distance. Fifty five telescoping CMARC models (11 shape changes and 5 angles of attack) are computed and stored in the aerodynamic database.
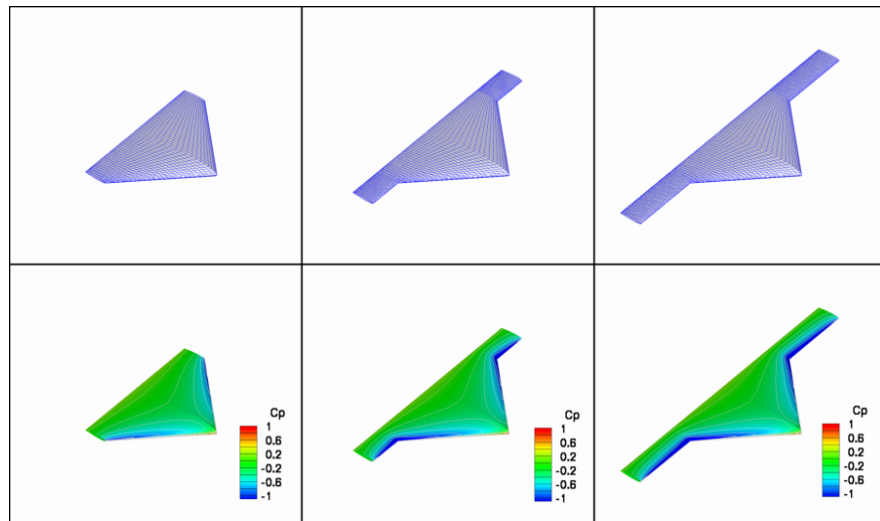

Figure A1: Meshes and coefficients of pressure for a telescoping wing. (Left: un-morphed, middle: 50% morphed, right: fully-morphed).

Figure A2 shows contour plots for the integrated coefficients for lift (C_L), pressure drag (C_{di}) and moment (C_m) as functions of angle of attack and telescoping distance.

Figure A3 shows the aerodynamic forces acting on the initial and the final configurations of the telescoping wing as used in VL and DYMORE analyses. The red color corresponds to forces at the center body section (stationary), while the blue color corresponds to the outer wing section (morphing section). At the top of the
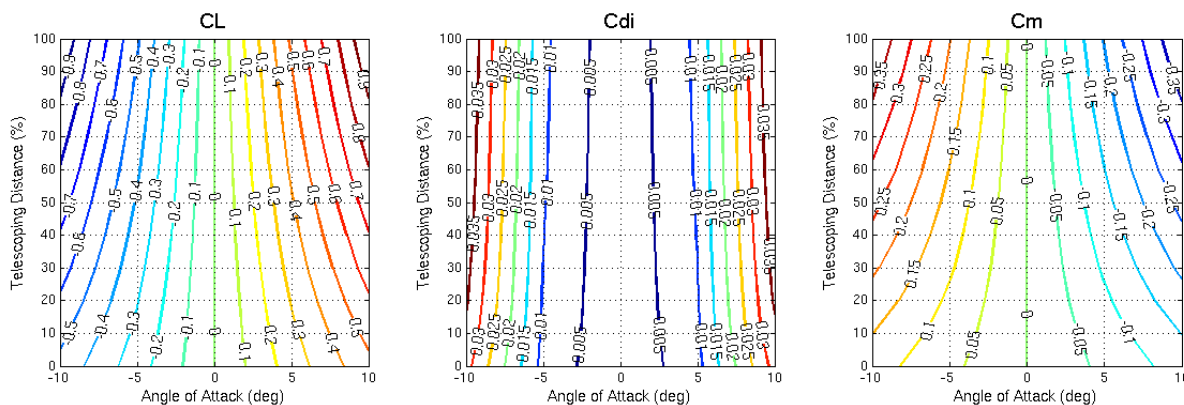

Figure A2: Lift, pressure drag, and moment coefficients for a telescoping wing.

figure is the un-morphed configuration and the fully-morphed configuration is shown at the bottom. For the un-morphed configuration, the outer telescoping section of the wing is inside the center body and has no forces acting on it. For the final morphed configuration, forces act on the center body and the outer wing. For DYMORE, the forces are applied to the points located along the wing quarter-chord line. Figure A4 shows the forces used in VL at various angles of attack and amount of telescoping. The red color corresponds to forces at the center body section (stationary), while blue corresponds to the outer wing section (morphing section). Because the structural elements in the center body section are larger, the nodal points on the center body section have larger nodal forces.
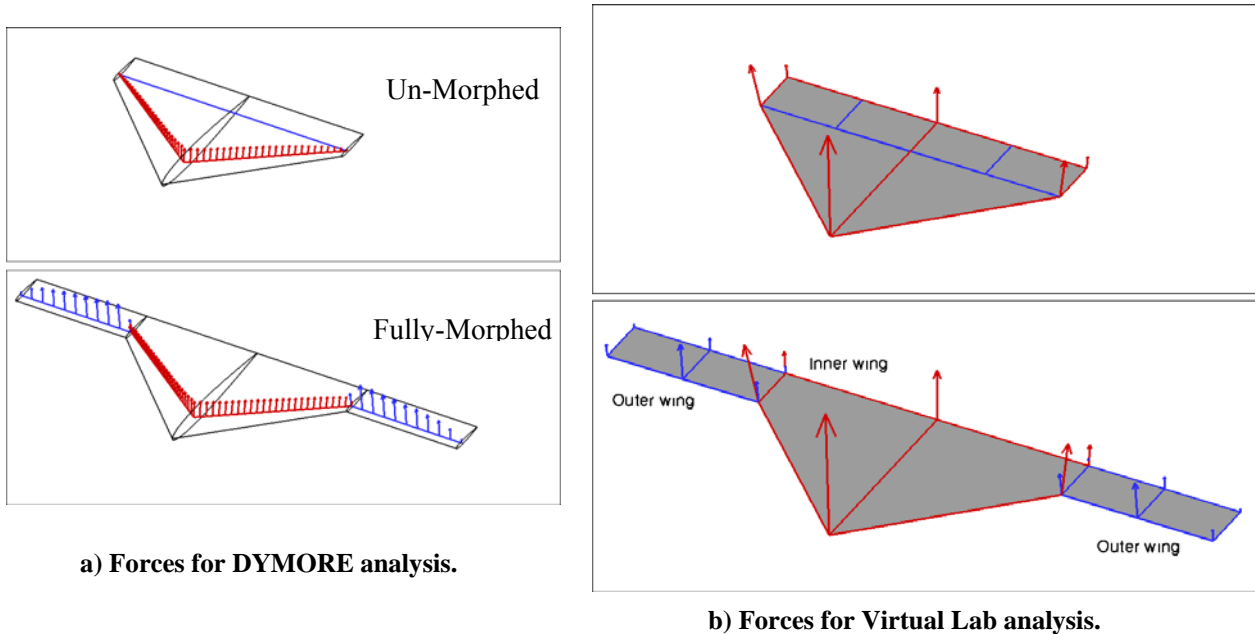

a) Forces for DYMORE analysis.

b) Forces for Virtual Lab analysis.

Figure A3: Initial and final forces for multibody dynamic analyses of a telescoping wing.
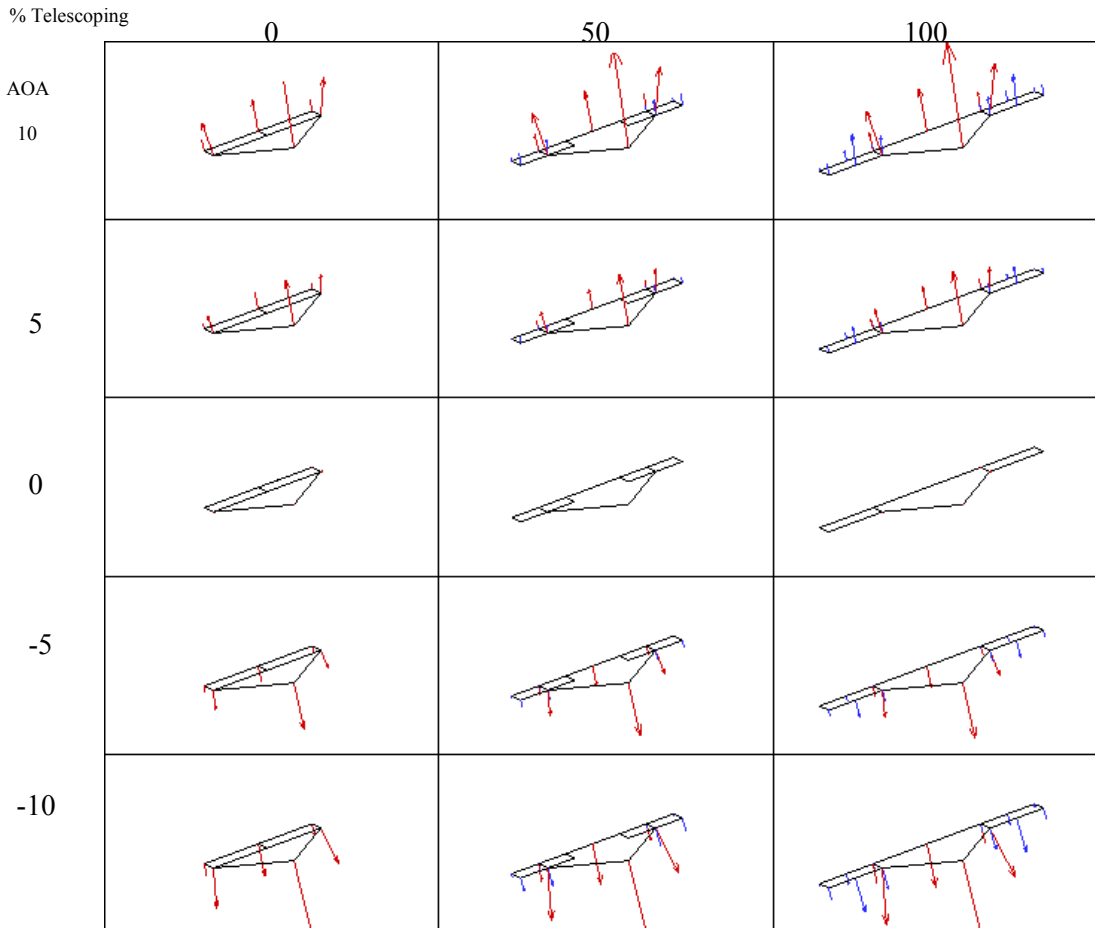
% Telescoping

Figure A4: Forces acting on telescoping configurations for VL analysis.

12.0 APPENDIX B: AERODYNAMIC RESULTS FOR THE FOLDING WING

Folding the wing's outer section, as shown in Fig. B1, reduces wing area and increases the effective sweep angle. These changes—area and sweep angle—create a vehicle that is optimum for two distinct missions. The planform for the folding model used here is shown in Fig. 5, and the corresponding parameters are listed in Tables 2 and 4. As before, all reference quantities are based on the un-morphed shape. Figure B1 shows the meshes and CMARC solutions for the folding wing at different stages of morphing. Similar to the telescoping case, MATLAB interpolates for the fold angle from its initial and final values and creates the aerodynamic database as a function of the angle of attack and the fold angle. Figure B2 shows the integrated coefficients for lift C_L, pressure drag C_{di}, and moment C_m as functions of angle of attack and fold angle. Figure B3 shows forces acting on VL model at various angles of attack and folding angles.
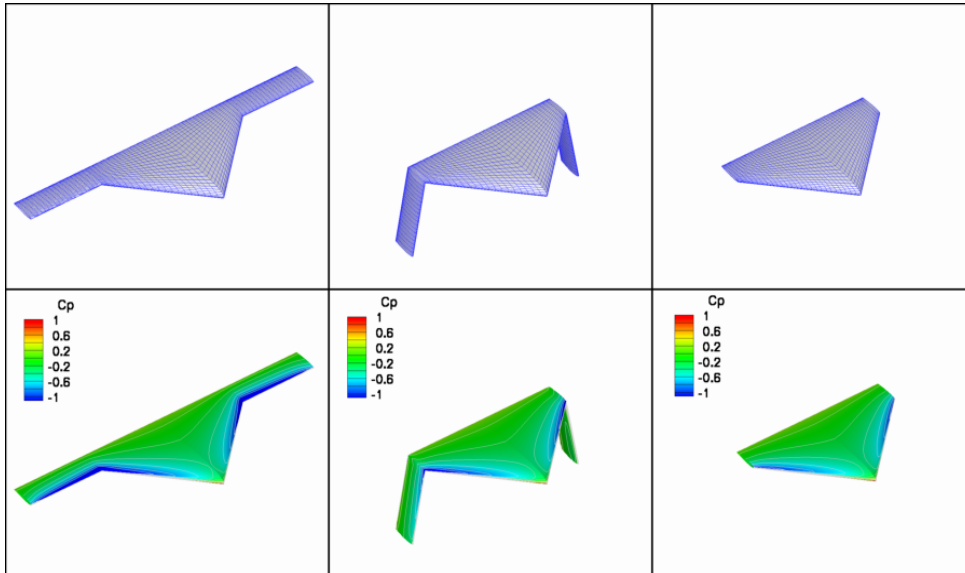
**Figure B1: Meshes and coefficients of pressure for a fold wing.
(Left: un-morphed, middle: 50% morphed, right: fully-morphed).**

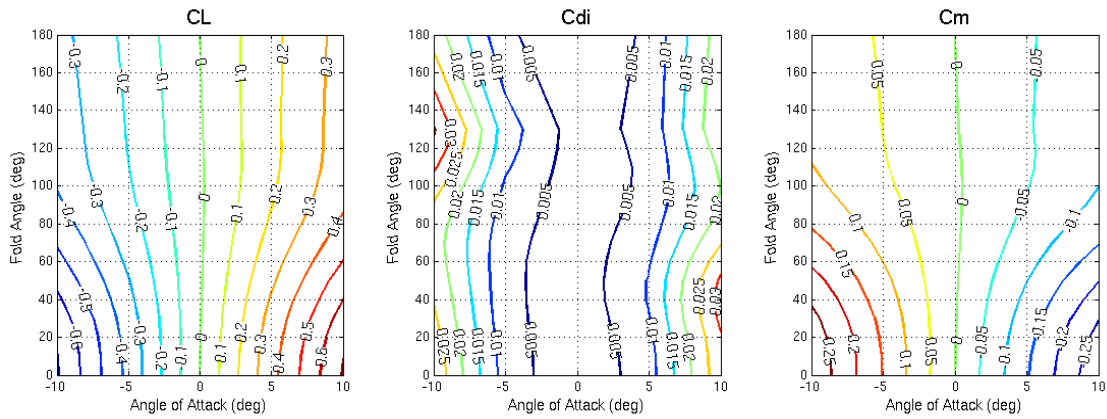**Figure B2: Lift, pressure drag, and moment coefficients for a folding wing.**
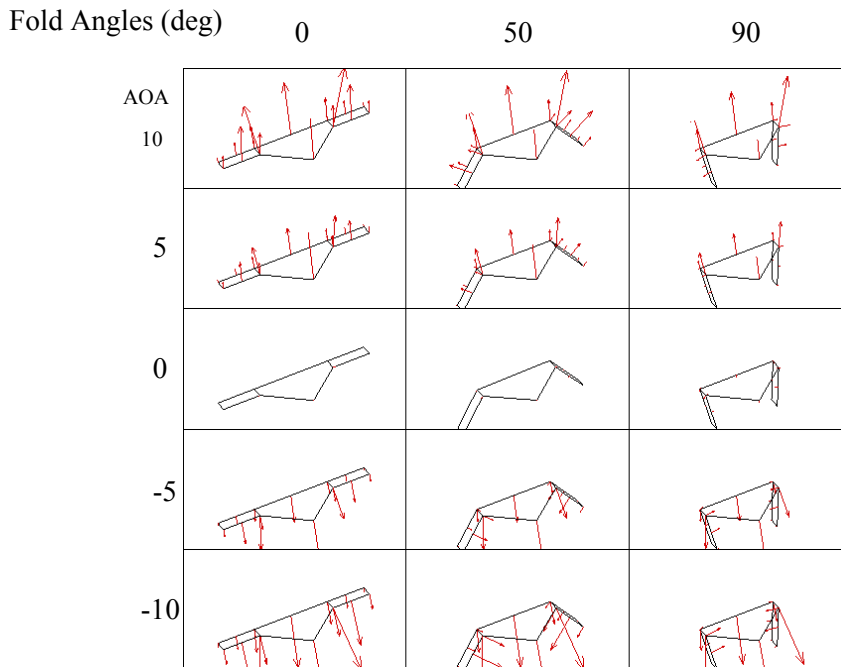
Fold Angles (deg)

Figure B3: Forces acting on folding configuration for VL.

13.0 APPENDIX C: AERODYNAMICS RESULTS FOR THE BAT-LIKE WING

Bat-like wing allows area and sweep angle changes that are optimum for two distinct missions. The planform for the bat-like model used here is shown in Fig. 5, and the parameters are listed in Tables 3 and 4. We used the initial root chord, the wing area, and the semi span for the aerodynamic reference quantities. Again, all reference quantities are based on the un-morphed shape. Figure C1 shows the meshes and CMARC solutions for the bat-like wing at different stages of morphing. MATLAB interpolates the wing planform parameters from its initial values to its final values of the leading edge sweep angle and creates an aerodynamic database, which is a function of the angle of attack and the sweep angles.
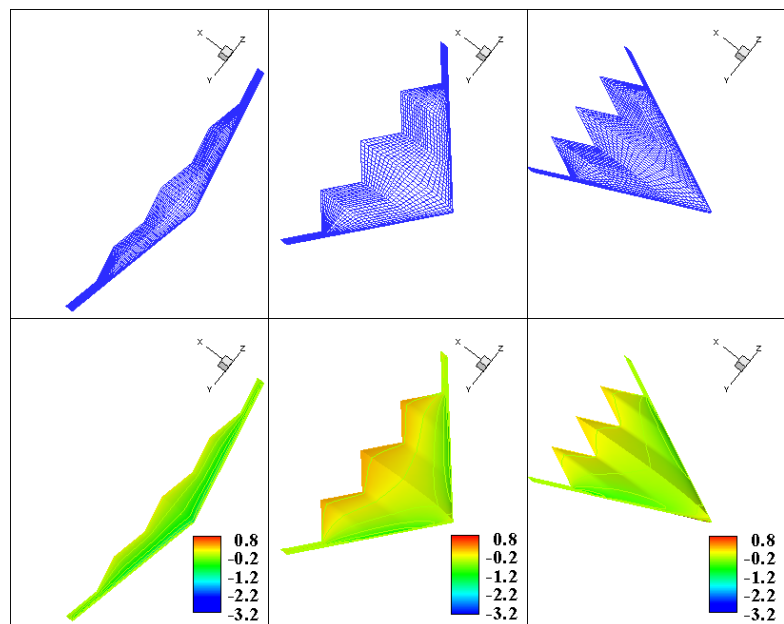

Figure C1: Meshes and coefficients of pressure for a bat-like wing.
(Left: un-morphed, middle: 50% morphed, right: fully-morphed).

Figure C2 shows the integrated coefficients for lift C_L, pressure drag C_{di}, and moment C_m as functions of angle of attack sweep angle. Figure C3 shows forces acting on DYMORE model at various angles of attack and sweep angle. The figure also highlights the beam element nodes and aerodynamic airstation points where aerodynamic forces and moments from MATLAB database are applied.
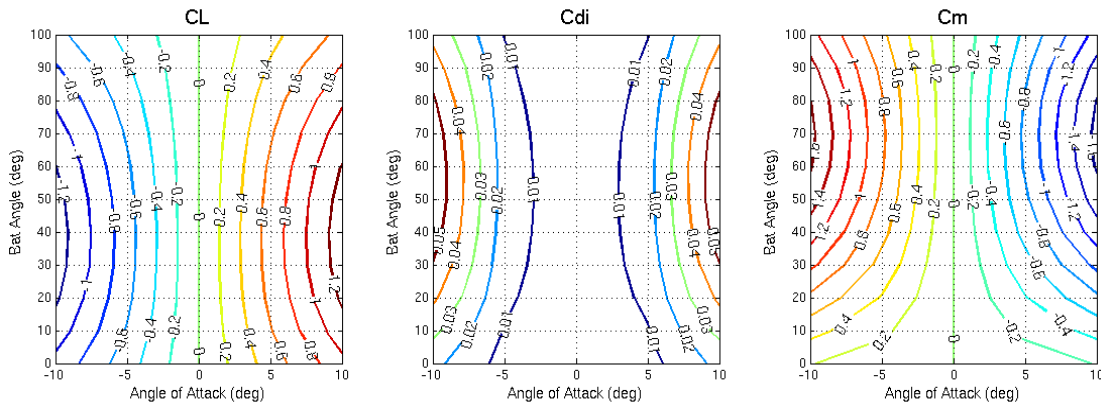

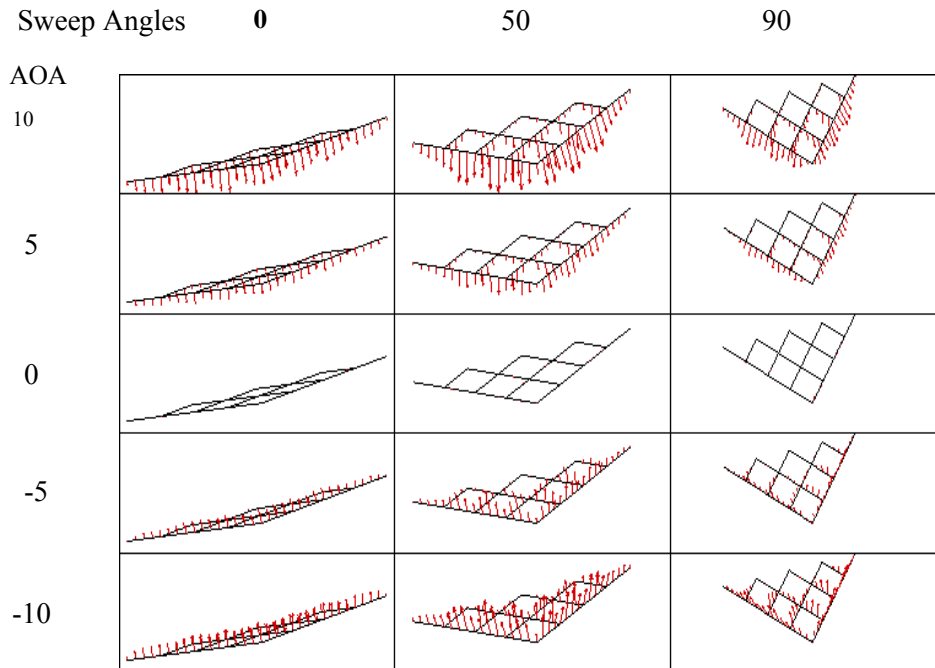**Figure C2: Lift, pressure drag, and moment coefficients for a bat-like wing.**

Figure C3: Forces acting on a bat-like wing configuration for DYMORE model.

14.0 REFERENCES

1. Bowman, J., Sanders, B., and Weisshaar, T., "Evaluating the Impact of Morphing Technologies on Aircraft Performance, AIAA-2002-1631, Denver, CO, April 2002.

2. Ramrkahyani, D. S., Lesieutre, G. A., Frecker, M., Bharti, S., "Aircraft Structural Morphing using Tendon Actuated Compliant Cellular Trusses," AIAA 2004-1728, Palm Springs, CA, April 2004.

3. Milholen, William E. and Owens, Lewis R., "On the Application of Contour Bumps for Transonic Drag Reduction," AIAA-2005-0462, Reno, NV, January 2005.

4. Davidson, J. B., Chwalowski, P., and Lazos, B.S., "Flight Dynamic Simulation Assessment of a Morphable Hyper-Elliptic Cambered Span Winged Configuration," AIAA-2003-5301, Austin, TX, August 2003.

5. Amprikidis, M., and Cooper, J. E., "Development of Smart Spars for Active Aeroelastic Structures," AIAA Paper 2003–1799, Norfolk, VA, April 2003.

6. McGowan, A. R., Cox, D .E., Lazos, B. S., Waszak, M. R., Raney, D. L., Siochi, E. J., Pao, S. P., "Biologically-Inspired Technologies in NASA's Morphing Project," SPIE Smart Structures and Materials Conference, v 5051, n 1, 2003.

7. Blondeau, J., Richeson, J., and Pines, D., "Design, Development and Testing of a Morphing Aspect Ratio Wing using an Inflatable Telescopic Spar," AIAA-2003-1718, Norfolk, VA, April 2003.

8. Kress, R. W., "Variable Sweep Wing Design," AIAA-1983-1051, Dayton, OH, March 1983.

9. Love, M. H., Zink, P. S., Stroud, R. L., Bye, D. R., Chase, C., "Impact of Actuation Concepts on Morphing Aircraft Structures," AIAA 2004-1724, Palm Springs, CA, April 2004.

10. Skillen, M. D. and Crossley, W. A., "Developing Morphing Wing Weight Predictors with Emphasis on the Actuating Mechanism," AIAA 2006-2042, Newport, RI, May 2006.

11. Samareh, J. A., Chwalowski, P., Horta, L. G., Piatak, D. J., McGowan, A. R., "Integrated Aerodynamic/Structural/Dynamic Analyses of Aircraft with Large Shape Changes," AIAA Paper 2007-2346, Honolulu, HI, April 2007.

12. Samareh, J. A., "Discrete Data Transfer Technique for Fluid–Structure Interaction" 18th AIAA Computational Fluid Dynamics Conference, Miami, FL, June 25-28, 2007, AIAA Paper 2007-4309.

13. Bauchau, O. A., "Computational Schemes for Flexible, Non-linear Multi-body Systems". Multibody System Dynamics, Volume 2, Number 2, pages 169-225, June 1998.

14. Ashby, D. L., "Potential Flow Theory and Operation Guide for the Panel Code PMARC_14," Ames Research Center, October 1999.

15. Miranda, L. R., Elliott, R. D., Baker W. M., "A generalized Vortex Lattice Method for Subsonic and Supersonic Flow Applications," NASA Contractor Report 2865, December 1977.

16 http://fun3d.larc.nasa.gov

17. Biedron, R. T, Thomas, J. L.,"Recent Enhancements to the FUN3D Flow Solver for Moving-Mesh Applications," AIAA Paper 2009-1360, Orlando, FL, January 2009.

18. Pirzadeh, S. Z.,"Advanced Unstructured Grid Generation for Complex Aerodynamic Applications," AIAA Paper 2008-7178, Honolulu, HI, August 2008.

19. Shen, J., Singleton, J.D., Piatak, D.J, "Multibody Dynamic Simulation and Experimental Investigation of a Model-Scale Tiltrotor." Presented at the American Helicopter Society 61st Annual Forum, Grapevine, TX, June 1-3, 2005.